Empirically Based Printer Model of Halftone Structure

Howard Mizes
Xerox Corp.
Webster, New York, USA

Abstract

A number of image quality metrics depend on the structure of the printed halftone dot. The dot structure depends in a complex way on the individual processes in a xerographic marking engine. This paper describes a model which reduces this complexity into a set of key parameters. The parameters are derived from microscopic optical measurements of the dot structure in the halftoned print on paper. The halftone printer model is written specifically for a single color separation, fast calculation, and physically based parameters. Given a fill pattern and a threshold value, it calculates the local image density as a function of position in a halftone supercell. The model has been applied to the appearance of partial pixels and to high frequency banding caused by irregularities in the raster optical scanner (ROS) beam spacing.

Introduction

A printer can be thought of as a device that transforms a digital image to a printed image. The digital image is transformed at each step of the print process so the printed image is modified from the digital image. An example of this transformation is dot gain, where the printed dots are larger than the dots of the digital image.

Many xerographic printers use a laser raster optical scanner (ROS) to create the latent image. The spot size and the laser intensity determine the size of the beam sweeping across the photoreceptor. The beam can be turned on and off with sub-pixel resolution to produce halftones with higher resolution than the spot size. Multiple beams can be swept across the printer simultaneously to increase throughput.

A good halftone design is free from artifacts. One example is contouring, which is an objectionably large change in optical density between two adjacent digital gray levels. A sweep from light to dark printed with this color separation would show an artificial boundary.

The appearance of the printed image is also sensitive to the exposure subsystem parameters. If the beams in a multiple beam imager are not evenly spaced, high frequency banding can be introduced into an image. If the spot size and exposure are too small, low area coverage will not print On the other hand, if the spot size and exposure are too large, the dot gain will be severe.

I developed a printer model to quantify the tradeoffs between the parameters and the halftone design. The model is derived from the physical characteristics of the xerographic printer. The model predicts the structure of a printed image on a scale that is smaller than the halftone dot. The model is controlled by a set of parameters that quantify how the individual subsystems affect the shape of the halftone dot. The parameters of the model are determined by measuring the microstructure of experimental halftones and fitting the unknown parameters of the model to the microstructure.

Printer models have been used previously to explore similar questions. For example, H. Sonnenberg explored the image degradation due to a finite laser beam and print process characteristics with a printer model.[1] R. Loce, W. Lama, and M. Maltz determined the magnitude of banding arising from vibrations that changed the velocity of the imaging media as it passed under the imager.[2] T. Pappas, J. Allebach, and D. Neuhoff use a printer model to predict the appearance of a halftone and use the model as a tool for halftone design.[3] J. Yi, R. Wells, and G. Kerby use a printer model to predict the appearance of a gray scale image over large areas as a means to test different halftone designs.[4]

I apply this model to exposure subsystem optimization. I calculate the high frequency banding introduced if the spacing between beams of a dual beam laser ROS are not exactly equal. I also calculate contouring that might be introduced if the partial pixels do not completely develop out.

Printer Model Algorithm

The model is similar to that published by Toyoshima *et al.*[5] A flowchart of my model is shown in figure 1. The printer model begins in step 1 with a digital image of the halftone. The parameters of the digital image include the halftone cell size, the addressability of the imager, and the gray level of the halftone to simulate. The area simulated is equal to the halftone cell size so periodic boundary conditions can be invoked and there are no edge effects. The digital pattern consists of a binary image with a resolution that of the addressability of the imager.

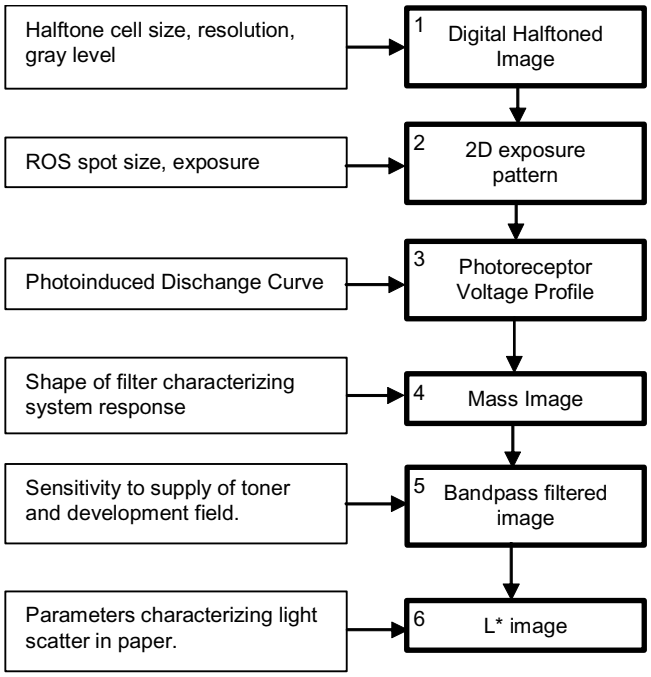

Figure 1. Empirically based printer model flowchart and model parameters.

In step 2, the digital image is converted to a two-dimensional exposure pattern. The points at which the laser turns on and off for each scan line are determined. The spot shape of the ROS is approximated by a two dimensional Gaussian function. The total exposure at each point is integrated analytically, giving an Error function in the cross process direction. The expression for exposure *e(x,y)* is

$$e(x,y)=\frac{E_0}{b_x b_y}\left\{erf\left[b_x(x-x_{off})\right]-erf\left[b_y(x-x_{on})\right]\right\}\times\exp-\left[b_y(y-y_{cen})\right]^2$$

where x and y are the cross process positions, x_{on} and x_{off} are the positions where the laser turns on and off, E_0 is the exposure, y_{cen} is the center of the beam in the cross process position, and *erf* is the error function. $b_x=2\sqrt{2}/w_x$ and $b_y=2\sqrt{2}/w_y$, where w_x and w_y are the full width half maximum widths size of the laser spot. The exposure image is calculated for a resolution smaller than the addressability of the imager, so details in the exposure pattern can be resolved.

In step 3, the exposure profile across the photoreceptor is converted to a voltage profile on the photoreceptor using a photo-induced discharge curve (PIDC). I approximate the PIDC with the following expression.[6]

$$V=\psi-\sqrt{\psi^2-V_c^2}+V_r,\psi=\left(V_0-V_c^2/V_0-e\cdot S\right)/2$$

In step 4, the photoreceptor voltage profile is converted to a toner mass profile by using the expression

$$m=\begin{cases}\alpha\left(1-e^{-\gamma(V_{d0}-V)/\alpha}\right), V>V_{d0}\\ 0, V<V_{d0}\end{cases}$$

where V is the voltage on the photoreceptor, V_{d0} is the voltage at which development begins, γ is the ratio between mass developed and voltage, and α is the maximum mass that can be developed.

In step 5, the image is spatially filtered in order to simulate the filtering in the xerographic subsystems. In a more complete xerographic model, the image is filtered at each xerographic subsystem. For example, charge spreading might occur during the exposure step, and toner might be scattered during development and transfer. However, the intent of this model is not to capture each subsystem contribution to dot gain, but instead to characterize how filtering changes the sensitivities. I choose to filter after the mass calculation by taking the Fourier transform of the two dimensional image, multiplying the transform by the modulation transfer function characteristic of the system, and inverting the transform to produce a filtered mass image. I parameterize the MTF with the following expression

$$M(f)=\frac{1}{1+(f/f_0)^n}$$

where f is the magnitude of the spatial frequency, and f_0 and n are adjustable parameters specifying the 50% cutoff of the filter and the sharpness of the cutoff.

In step 6, the developed mass is converted to the luminosity of the image on paper. Scattering of light within the paper gives an optical dot gain which is parameterized with the Yule-Nielsen equations.[7] However, the application of the Yule-Nielsen equations gives an average reflectance but does not predict the local structure. Instead, we use a technique proposed by Arney, Engeldrum, and Zeng[8] to predict the dot microstructure.

Experimental Parameterization of Optical Gain

In the experimental technique proposed by Arney *et al*, high resolution images of a series of halftones are measured. The gray level histogram is calculated at each halftone level. The histogram has two peaks, one corresponding to the halftone dots and one corresponding to the paper. The gray levels at which the peaks occur decrease as a function of toner area coverage because less light can enter the paper.

Following Arney *et al*, we capture this behavior with the following equations

$$r(x,y)=r_{m0}+(r_{m1}-r_{m0})\left(1-e^{-m(x,y)/r_{m2}}\right)$$
$$r_{m0}=r_{p0}+r_{p1}\langle m(x,y)\rangle$$

The units are reflectance in the units of the camera system. $m(x,y)$ is the model mass profile. r_{p0} is the reflectance of paper and r_{p1} is the rate this reflectance decreases as the paper is covered with toner. r_{m1} is the reflectance of the image at high area coverage.

To convert the high resolution reflectance profile to CIELAB luminosity, we use the expression.

$$L = 116\left(\frac{< r(x,y) > -L_{r1}}{L_{r0}}\right)^{1/3} - 16$$

where L_{r1} and L_{r0} are chosen experimentally so the high resolution imager response matches the spectrophotometer response.

Image Simulation with Model

Figure 2 shows the evolution of a digital bitmap to a simulated image. In figure 2(a) black represents a binary pixel which should be image and white represents a binary pixel that should be left blank. This image is converted into an exposure pattern illustrated in 2(b). Then using the PIDC shown in figure 2(c), the image is converted into a voltage profile 2(d). Following this step, the development curve shown in figure 2(e) is used to convert the image into a mass profile shown in figure 2(f). A low pass filter simulates the blurring of the image in figure 2(g). The equations of Arney et all are used to convert the mass profile into a predicted image in figure 2(h).

Microstructure Comparison Between Theory and Experiment

Figure 3 shows a typical image of a halftone taken with a high resolution camera. Each halftone dot appears different due to the randomness of toner deposition. This randomness dominates the image and makes a qualitative comparison between the experimental measurement and the model difficult.

To make a comparison with experiment, I identify the unit cell in figure 3(a) (shown as the overlaid rectangle). I sum all the imaged unit cells and average the result pixel by pixel, shown in figure 3(b). An alternative but equivalent way to calculate the same image is to take the 2D Fourier transform of figure 3a. It will show an array of peaks in two dimensions caused by the periodicity of the image. Setting the Fourier transform to zero in all regions except at these peaks eliminates nonperiodic features and also produces figure 3(b).

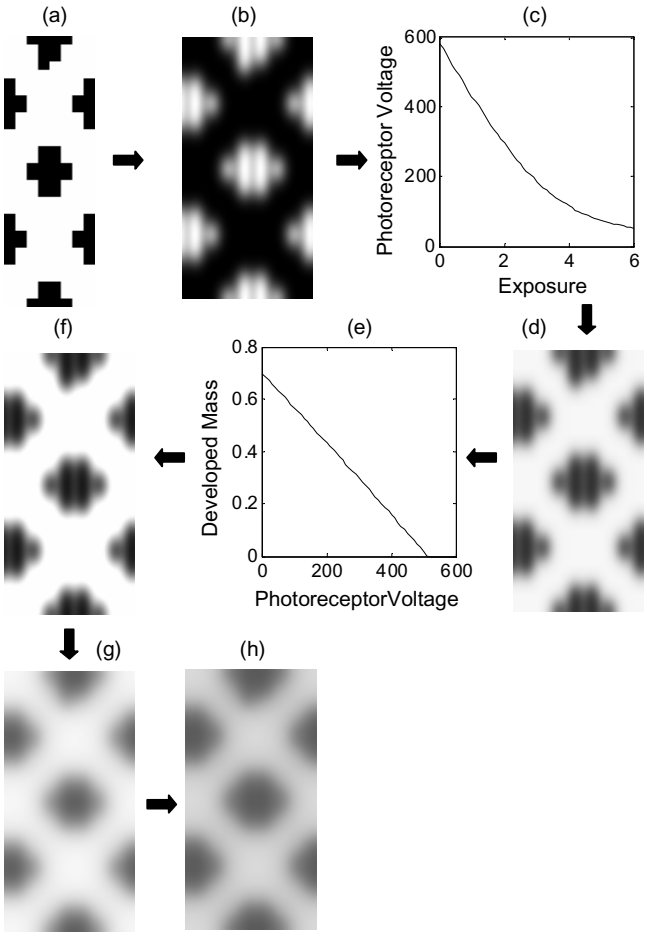

Figure 2. Transformation of digital image to printed image (a) bitmap image, (b) exposure pattern, (c) PIDC, (d) photoreceptor voltage, (e) development curve, (f) mass image, (g) blurred mass image, (h) appearance of image on paper.

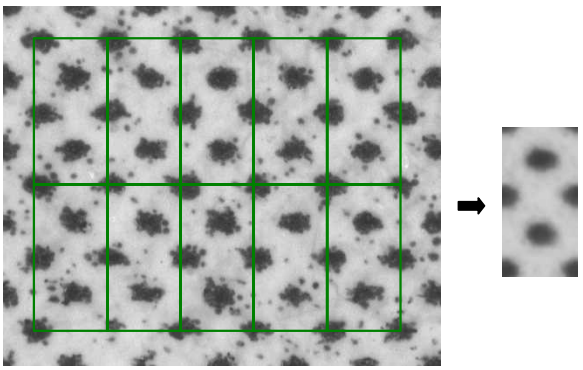

Figure 3. Technique to average over toner deposition randomness.

Figure 4 shows a side by side comparison of the model and the experiment at a series of area coverages. The decreased light reflectance from the paper is seen both experimentally and in the images. Figure 5 further quantifies these results. A series of three curves are shown. The center curve is the tone reproduction curve (TRC), the average luminosity's dependence on input area coverage. The upper curve is the dependence of the maximum bare paper reflectance on input area coverage, and the lower curve is the dependence of the minimum reflectance at the dot center on area coverage.

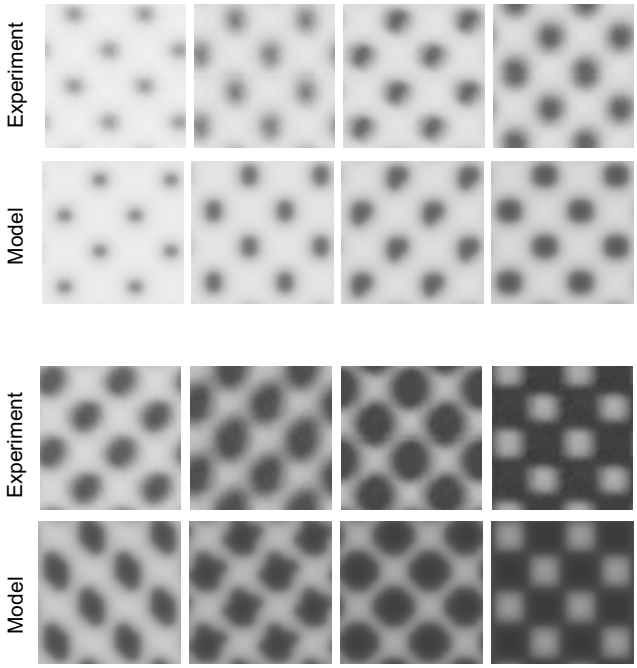

Figure 4. Model prediction vs. experimental image for various area coverages.

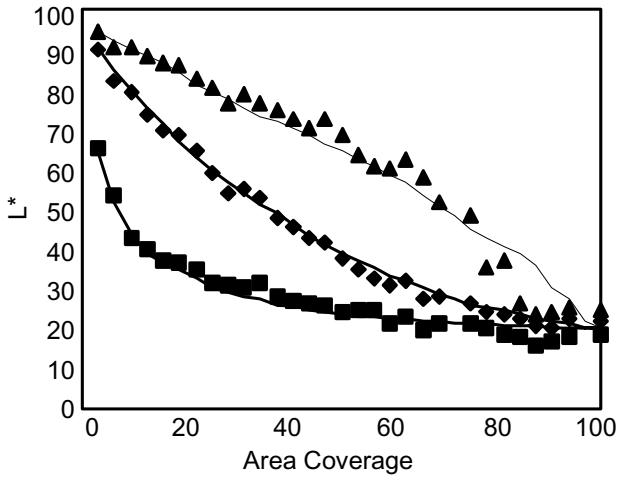

Figure 5. Measured and predicted luminosity. Dot center (squares), paper region (triangles), and average (diamonds).

Halftone Sensitivity to ROS Parameters

The luminosity will depend on both the spot size of the ROS and its exposure. Large spot sizes and high exposures will increase the discharge of the photoreceptor. The spot size may change as the ROS beam sweeps from one side of the photoreceptor to the other side of the photoreceptor. If the change is significant enough, this may lead to a color shift from one side of the paper to the other.

Figure 6 shows the dependence of L* as predicted by the model for a particular set of parameters. I plot L* vs. (a) a change in the spot size in the process direction, (b) a change in the spot size in the cross process direction, and (c) a change in the exposure. There are no regions where the relative sensitivity between adjacent halftone levels differs significantly, so one can conclude that a change in the exposure subsystem parameters over this range will not introduce artifacts.

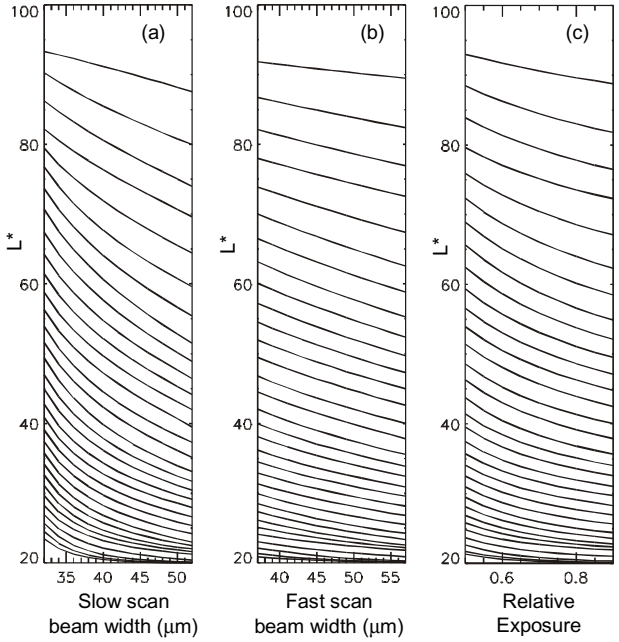

Figure 6. Model prediction for luminosity changes with exposure subsystem parameters.

Dual Beam Spacing and Banding

To increase the speed of writing, some printers separately control two beams as they sweep across the photoreceptor. The beams must be spaced by an integral number of pixels, or the printed pattern will have scan lines that are unequally spaced and high frequency banding will be introduced into the print. For a dual beam laser, the high frequency banding will be at such a high frequency it will not be perceptible. However, for some halftones, the high frequency will beat with the halftone pattern. This beating may introduce a banding at a lower frequency that will be perceptible.

The empirical model can be a useful tool in determining the latitude required for the spacing between the laser beams. One can calculate the banding by averaging the predicted image along the cross process direction and then taking the Fourier transform of this average. If there is a dual beam spacing error, the Fourier transform will have a peak at the period between the two beams as well as peaks at any beating frequencies with the halftone. Figure 7 plots the amplitude of the banding at the dual beam spacing as a function of the spacing error between the lasers. The model can also be used to explore the root causes and how banding is mitigated by other subsystem parameters.

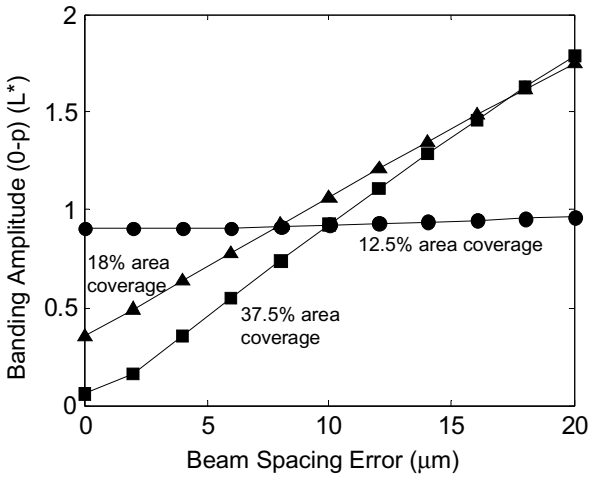

Figure 7. Dependence of high frequency banding amplitude on beam spacing error.

Partial Pixels Effects

The ROS can be controlled so that the addressability in the fast scan direction is higher than the spacing between pixels. This capability gives more control over the growth of the halftone dots and thus the opportunity for higher quality halftone screens. However, this capability also gives the potential for the introduction of artifacts which the printer model can predict.

Figure 8 shows three structures for a halftone that can be designed if this capability exists along with the model prediction for the appearance of the dot. The center image and the right image show two possibilities of how to increase the size of the dots in the left image for the next level. The center image adds a partial pixel to a different scan line, while the right image increases the width of a scan line.

The model predicts a significant difference in the luminosity for the two halftones. When a partial pixel is added in a new scan line, the laser is turned on for so short of a time, the photoreceptor does not sufficiently discharge and no new toner can be developed. However, increasing the time the laser is turned on for one of the scan lines increases the developed toner approximately equal to the width of the on portion of the scan line.

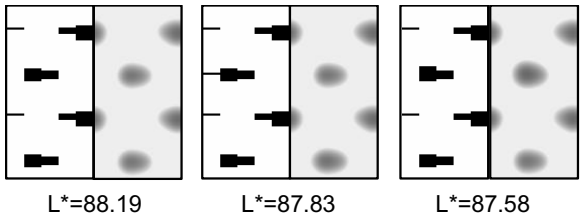

Figure 8. Predicted luminosity for different arrangements of partial pixels.

Figure 9 shows a prediction of the TRC for an experimental dot containing partial pixels introduced in a suboptimal way along with an experimental measurement of the TRC. The model predicts a number of features that are seen experimentally. It predicts that area coverage at which the TRC rolls over and development occurs. It also predicts structure in the TRC that is observed near an area coverage of 40%. The table in the figure gives a quantitative comparison between the model predictions and the experimental measurements. The agreement of L* at low and high area coverage is good because the model parameters were adjusted to fit the experimental data in this region. However, the initial increase of the TRC at the 9th gray level and the structure in the TRC around 40% is an outcome of structure of the model.

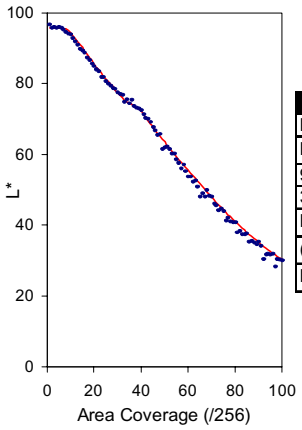

	Experiment	Model
Lpaper	95.77	95.77
L_9	94.12	94.98
9th dot width	28	26.4
32nd dot width	70	51.0
L_{40}	72.24	72.24
$(L_{32}-L_{40})/(L_{40}-L_{48})$	0.524	0.528
L_{96}	32.0	32.0

Figure 9. Predicted and measured structure in a TRC.

Conclusions

Designing a well behaving printer requires some understanding of the interplay between the exposure subsystem and the halftone design. The empirical printer model described in this paper can act as this tool. The exposure, spot size, and beam spacing are accurately modeled so an accurate exposure pattern is calculated. The responses of the other subsystems to this exposure pattern are modeled in a simple way. By simplifying these responses, significant features of the printer, such as its

resolution or where on the PIDC the printer is operated, can be modeled to find the best operating point and the reasons other operating points are not as good. The model can also be used as a tool to determine the sensitivities of image quality metrics to exposure subsystem parameters and how different halftone dot designs can mitigate these sensitivities.

References

1. H. Sonnenberg, "Laser-Scanning Parameters and Latitudes in Laser Xerography", Appl. Opt. 21, 10, 1745-1751 (1982).
2. R. P. Loce, W. L. Lama, and M. S. Maltz, "Modeling Vibration-Induced Halftone Banding in a Xerographic Laser Printer", J. Electron. Imaging 4, 11 pp. 48-61 (1995).
3. T. N. Pappas, J. Allebach, and D. L. Neuhoff, "Model Based Digital Halftoning", IEEE Signal Processing Magazine, 20 pp. 14-27 (2003).
4. J. Yi, R. Wells, and G. Kerby, "Efficient Grayscale Rendering of Large Images Using a Signal Processing Modeling and the Arctangent Function", NIP19, pp. 830-835 (2003).
5. T. Toyoshima, T. Iwamatsu, N. Azuma, S. Nishio, and Y. Matoh, "Optimization of the Image Profile Transform in High Resolution Electrophotography", Proceedings of IS&T NIP16 Conference, 2000, p. 303-306.
6. A. R. Melnyk and D. M Pai, Proceedings of SPIE/SPSE Symposium on Electronic Imaging, Santa Clara, pp. 141, edited by J. Gaynor, SPIE, Bellingham, WA 1990.
7. J. A. Yule and W. J. Nielsen, TAGA Proc. p. 65 (1951).
8. J. S. Arney, P. G. Engeldrum, and H. Zeng, An expanded Murray-Davies model of toner reproduction in halftone imaging, J. Imaging Sci. Technol. 39: 502 (1995).

Biography

Howard Mizes received his BS degree in Physics from the University of California at Los Angeles in 1983, and his Ph.D. degree in Applied Physics from Stanford University in 1988. Since 1988, he has been with Research and Technology at Xerox Corporation, where he is a Principal Scientist. Dr. Mizes' research has been primarily focused on understanding and controlling the process physics of xerographic printing, and quantifying and improving the resulting image quality. He has worked in the areas of charge transport and contact charging, particle adhesion measurements and modeling, and experimental probes of the xerographic development process. His image quality work has focused on improving the spatial uniformity of the printed page. e-mail: hmizes@crt.xerox.com